



This is the accepted manuscript made available via CHORUS. The article has been published as:

Anisotropic in-plane heat transport of Kitaev magnet math xmlns="http://www.w3.org/1998/Math/MathML">mrow>msub>mi>Na/mi>mn>2/mn>/msub>msub>mi>Co/mi>mn>2/mn>/msub>msub>mi>TeO/mi>mn>6/mn>/msub>/mrow>/math>

Shuangkui Guang, Na Li, Qing Huang, Ke Xia, Yiyan Wang, Hui Liang, Yan Sun, Qiuju Li, Xia Zhao, Rui Leonard Luo, Gang Chen, Haidong Zhou, and Xuefeng Sun

Phys. Rev. B **109**, 024419 — Published 16 January 2024

DOI: 10.1103/PhysRevB.109.024419

Anisotropic in-plane heat transport of Kitaev magnet $Na_2Co_2TeO_6$

Shuangkui Guang,[1] Na Li,[2,1] Qing Huang,[3] Ke Xia,[1] Yiyan Wang,[2] Hui Liang,[2] Yan Sun,[2] Qiuju Li,[4] Xia Zhao,[5] Rui Leonard Luo,[6] Gang Chen,[6,*] Haidong Zhou,[3,†] and Xuefeng Sun[2,1,7,‡]

[1] *Department of Physics, University of Science and Technology of China, Hefei, Anhui 230026, People's Republic of China*
[2] *Anhui Key Laboratory of Magnetic Functional Materials and Devices, Institute of Physical Science and Information Technology, Anhui University, Hefei, Anhui 230601, People's Republic of China*
[3] *Department of Physics and Astronomy, University of Tennessee, Knoxville, Tennessee 37996-1200, USA*
[4] *School of Physics and Optoelectronics, Anhui University, Hefei, Anhui 230061, People's Republic of China*
[5] *School of Physics Sciences, University of Science and Technology of China, Hefei, Anhui 230026, People's Republic of China*
[6] *Department of Physics and HKU-UCAS Joint Institute for Theoretical and Computational Physics at Hong Kong, The University of Hong Kong, Hong Kong, People's Republic of China*
[7] *Collaborative Innovation Center of Advanced Microstructures, Nanjing University, Nanjing, Jiangsu 210093, People's Republic of China*

(Dated: December 8, 2023)

We report a study on low-temperature heat transport of Kitaev magnet $Na_2Co_2TeO_6$, with the heat current and magnetic fields along the honeycomb spin layer (the *ab* plane). The zero-field thermal conductivity of κ^a_{xx} and κ^{a*}_{xx} display similar temperature dependence and small difference in their magnitudes; whereas, their magnetic field (parallel to the heat current) dependence are quite different and are related to the field-induced magnetic transitions. The $\kappa^a_{xx}(B)$ data for $B \parallel a$ at very low temperatures have an anomaly at 10.25–10.5 T, which reveals an unexplored magnetic transition. The planar thermal Hall conductivity κ^a_{xy} and κ^{a*}_{xy} show very weak signals at low fields and rather large values with sign change at high fields. This may point to a possible magnetic structure transition or the change of the magnon band topology that induces a radical change of magnon Berry curvature distribution before entering the spin polarized state. These results put clear constraints on the high-field phase and the theoretical models for $Na_2Co_2TeO_6$.

I. INTRODUCTION

Kitaev model is an exactly solvable spin model that supports Z_2 spin liquid with gapless Majorana excitations [1]. In the presence of magnetic fields, the Kitaev model can further support gapped spin liquid with gapless and chiral Majorana mode that gives rise to half-quantized thermal Hall conductance. The presence of Kitaev interaction in the spin-orbit-coupled $J = 1/2$ honeycomb magnets with $5d$ iridium ions (Ir^{4+}) [2] and $4d$ ruthenium ions (Ru^{4+}) was suggested later [3]. Unfortunately, most of the relevant honeycomb irridates and even α-$RuCl_3$ are well ordered at low temperatures [4]. α-$RuCl_3$ in the magnetic field seems to support the half-quantized thermal Hall transport, that may be compatible with the gapped Kitaev spin liquid [5–7]. Nevertheless, the actual ground state of α-$RuCl_3$ in magnetic fields still needs further scrutiny. On the material's side, there were some efforts that proposed candidate Kitaev materials beyond the $4d/5d$ contexts, and these include the $4f$ rare-earth Kitaev magnets and the $3d$ transition metal Kitaev magnets. Along the line of the $3d$ transition metal Kitaev magnets, several honeycomb cobalt compounds such as $Na_2Co_2TeO_6$, $Na_3Co_2SbO_6$, and $BaCo2(AsO_4)_2$ were proposed and studied [8–11].

The question about the Kitaev interactions in these Co-based materials, especially for $BaCo_2(AsO_4)_2$, has been raised in Refs. 12 and 13. It was found that the experimental results based on neutron scattering in $BaCo_2(AsO_4)_2$ can be consistently accounted for by the XXZ model on the first and third neighbors but not by the more anisotropic spin model with Kitaev interactions and other pseudo-dipole interactions. It is then further remarked that, the frustration in $BaCo_2(AsO_4)_2$ is mainly from the competing first and third interaction, rather than from the Kitaev-related anisotropic interaction. Likewise, one could raise the same question for the honeycomb cobalt $Na_2Co_2TeO_6$ since no consensus has been reached concerning the microscopic models [14–19]. Here with our comprehensive thermal transport measurements, we are able to address this question, and the experimental results point to more anisotropic spin interactions.

In this work, we study the in-plane thermal conductivity and thermal Hall conductivity of $Na_2Co_2TeO_6$ with both the heat current and magnetic field along the a or $a*$ axis. The magnetic field dependence of both thermal conductivity and thermal Hall conductivity display in-plane anisotropic behaviors. This is a strong indication of the intrinsic anisotropic nature of the spin interactions

* gangchen@hku.hk
† hzhou10@utk.edu
‡ xfsun@ahu.edu.cn

as a Kitaev material. In addition, the low-temperature $\kappa_{xx}^{a}(B)$ with a-axis field exhibits an anomaly at 10.25–10.5 T that is argued to be associated with an unexplored magnetic structure transition. We further provide a physical reasoning about the Berry curvature properties based on the contents of κ_{xx} and κ_{xy}. This way of reasoning may be well generalized to other quantum magnets with the cooperative responses in κ_{xx} and κ_{xy} with respect to the external magnetic fields.

II. EXPERIMENTS

High-quality single crystals of $Na_2Co_2TeO_6$ were grown by a flux method as previous reported [20]. Two thin-plate shaped crystals with size of $6.30 \times 2.17 \times 0.053$ mm^3 and $5.20 \times 2.10 \times 0.047$ mm^3 were used for heat transport measurements. The heat current and magnetic field were applied along the longest dimension of these two samples, which is the a-axis and $a*$-axis direction, respectively. The longitudinal thermal conductivity and thermal Hall conductivity were measured simultaneously by using the standard steady-state technique with "one heater, three thermometers" [21]. Heat current and magnetic field were applied along the a or $a*$ axis and they were always parallel or antiparallel to each other. The longitudinal and transverse temperature gradients were measured by three in-situ calibrated RuO_2 thermometers. The measurements were carried out in a ^{3}He refrigerator equipped with a 14 T magnet. It should be pointed out that since the planar thermal Hall effect of $Na_2Co_2TeO_6$ was found to be rather weak, each κ_{xy} data point displayed in this paper was the averaged value of data measured for more than five times and the corresponding standard deviation of averaging the data points was used as error bar.

III. RESULTS AND DISCUSSIONS

Figure 1 shows the temperature dependence of the longitudinal thermal conductivity κ_{xx}^{a} and κ_{xx}^{a*}, measured in zero field and with heat current along the a axis and the $a*$ axis, respectively. $Na_2Co_2TeO_6$ is known to have a zigzag [22, 23] or triple-q [25, 37] antiferromagnetic (AF) order below the Néel temperature ($T_N \approx 27$ K), followed by two possible spin re-orientation transitions around 16 K and 6 K. Though the $\kappa_{xx}(T)$ data shows no obvious anomaly around 27 K and 16 K, similar to the reported results [26], a slope change below 6 K can be related to the spin re-orientation. At subkelvin temperatures, the $\kappa_{xx}(T)$ exhibits a roughly $T^{1.2}$ behavior that is significantly weaker than the expected T^3 behavior of phonons and indicates the existence of magnetic scattering of phonons. Assuming the purely phononic contribution to thermal conductivity, the phonon mean free path can be estimated. As shown in the inset to Fig. 1, the ratios of the phonon mean free path to the averaged sample

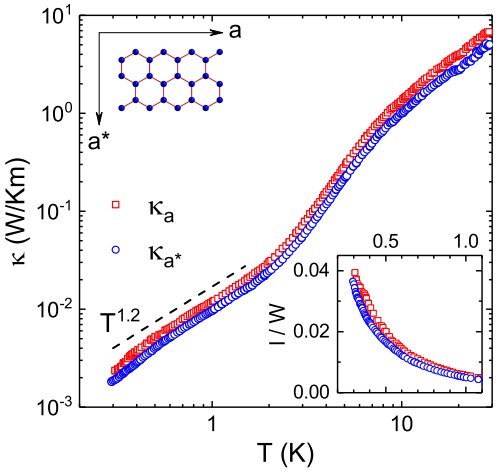


FIG. 1. Temperature dependence of the longitudinal thermal conductivity κ_{xx}^{a} and κ_{xx}^{a*} of $Na_2Co_2TeO_6$ single crystals, measured in zero magnetic field and with heat current along the a axis (the zigzag direction) and the $a*$ axis (the Co-Co bond direction), respectively. The dashed line indicates a $T^{1.2}$ dependence of κ at low temperature. The inset demonstrates the direction of a axis and the $a*$ axis in the honeycomb layer of Co^{2+}, and the ratio of estimated phonon mean free path to the averaged sample width.

width are much smaller than 1 even at $T < 1$ K, indicating the existence of microscopic phonon scattering effect at such low temperatures. It is notable that at zero field the κ_{xx}^{a} and κ_{xx}^{a*} have similar temperature dependence with slight difference in their magnitudes; whereas, they exhibit rather different magnetic field dependence for the in-plane fields.

Figures 2(a-d) show the magnetic field dependence of κ_{xx}^{a*} with the heat current and magnetic field along the $a*$ axis at several selected temperatures from 0.375 to 3.2 K. It is found that $\kappa_{xx}^{a*}(B)$ shows a sharp jump at $B_{a*1} \sim 6.25$ T with increasing field , and subsequently exhibits two minima at $B_{a*2} \sim 7.5$ T and $B_{a*3} \sim 10$ T before the saturation. According to the previous magnetization results [27], the B_{a*1} corresponds to a first-order magnetic transition and shifts to lower field with increasing temperature. Meanwhile, a large hysteresis occurs in $\kappa_{xx}^{a*}(B)$ at $B < B_{a*1}$. The rather sharp minima of $\kappa_{xx}^{a*}(B)$ at B_{a*2} and B_{a*3} indicate two magnetic transitions, which is compatible with the recent inelastic neutron scattering measurements that revealed a field-induced intermediate magnetic state with partially polarized spins between 7.5 T and 10 T with magnetic field along the $a*$ axis [28]. All these results are consistent with our previous data measured at lower temperatures down to millikelvin temperatures [29].

Figures 2(e-h) show the planar thermal Hall conductivity κ_{xy}^{a*} as a function of magnetic field at above selected temperatures. For all selected temperatures, there is no discernible κ_{xy}^{a*} signal at $B < B_{a*3}$ and some sizeable thermal Hall signal ~~appears~~ seems to appear at higher magnetic fields. Whereas, an obvious feature was ob-

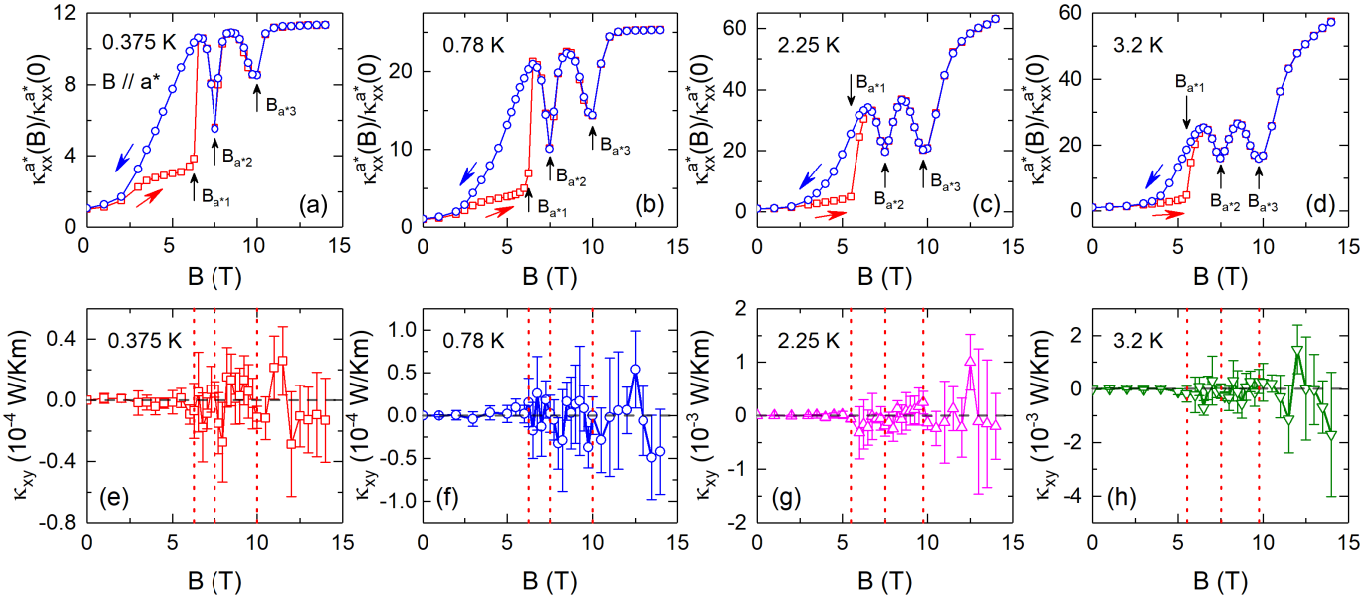


FIG. 2. Longitudinal thermal conductivity κ_{xx}^{a*} and thermal Hall conductivity κ_{xy}^{a*} of $Na_2Co_2TeO_6$ single crystals as a function of magnetic field with magnetic field and heat current applied along the $a*$ axis. (a-d) Isotherm curves of the κ_{xx} with respect to the zero-field value as a function of magnetic field at 0.375 K, 0.78 K, 2.25 K and 3.2 K, respectively. The red and blue arrows indicate the process of applying magnetic field and the black arrows indicate the critical fields (B_{a*1}, B_{a*2} and B_{a*3}) as mentioned in the main text. An obvious hysteresis can be observed at $B < B_{a*1}$. (e-h) Magnetic field dependence of thermal Hall conductivity κ_{xy} at 0.375 K, 0.78 K, 2.25 K, and 3.2 K, respectively. Each data point is the averaged result from the repeated measurements for more than five times, the error bars represent the standard deviation. The red dot line indicates the positions of B_{a*1}, B_{a*2} and B_{a*3}.

served in the high-field region above B_{a*3}. That is, the κ_{xy}^{a*} signal first shows a peak with positive signal and then changes the sign at higher fields. This high-field feature is shared by the data at all selected temperatures, indicating an intrinsic narrow region with the positive κ_{xy} before entering the high-field fully polarized state. It should be pointed out the high-field κ_{xy}^{a*} signal is rather weak at such low temperatures from 0.375 to 3.2 K since the error bars are quite large. However, these high-field might be true since more pronounced κ_{xy}^{a*} signals with relative smaller error bars was observed at higher temperature of 7.8 K (see the Supplemental Material).

The planar thermal Hall conductivity and thermal conductivity was recently studied at higher temperature region of 2–30 K by Takeda *et al.* [30]. It is interesting to compare their results and ours. First, our $\kappa_{xx}^{a*}(B)$ data display much sharper minima at B_{a*2} and B_{a*3}, indicating better sample quality. Second, although their low-field $\kappa_{xy}^{a*}(B)$ data are also almost zero, they show a sharp minimum with negative values at B_{a*1}. This feature is absent in our results. Third, their high-field $\kappa_{xy}^{a*}(B)$ data at 2 and 5 K also exhibits rather complicated behavior with sign changes, which is similar to ours.

To clarify the most significant difference in the $\kappa_{xy}^{a*}(B)$ data at B_{a*1} between two groups, we took very careful checks on the measurements and noticed that it may be related to the rather long relaxation time of temperature gradients at this critical field. For this checking measurement, particularly at B_{a*1} and at 0.78 K, the temperature gradients were measured with different waiting times after applying the heat current. At this temperature and in 0–14 T fields, usually several minutes are enough to establish the equilibrium heat flowing state. However, at B_{a*1} we found that the relaxation time is much longer. First, we carried out a set of measurement with long waiting time. Figure 3(a) shows the $\kappa_{xx}^{a*}(B)$ data for $+B$ and $-B$ fields and Fig. 3(e) shows the corresponding $\kappa_{xy}^{a*}(B)$ data, for which all the temperature gradients were recorded with long enough waiting time ($>$ 30 minutes) after applying the heat current. Figures 3(b) and 3(f) show the longitudinal and transverse temperature gradients, which are stable enough and only weakly fluctuating with flat based lines. In this case, the κ_{xx}^{a*} data at -6.5 T (several times measurements) are indistinguishable from that at 6.5 T; accordingly, the obtained κ_{xy}^{a*} data at 6.5 T are small and the $\kappa_{xy}^{a*}(B)$ curve does not show any anomaly at this critical field. Second, at -6.5 T the temperature gradients were recorded with usual waiting time (several minutes) after applying the heat current, as shown in Fig. 3(d) and 3(h). In this case, the temperature gradients are not stable enough although the shifts of temperature gradients are very weak. Accordingly, the κ_{xx}^{a*} data at -6.5 T are slightly smaller than that at 6.5 T and the obtained κ_{xy}^{a*} data show rather large negative values, as shown in Fig. 3(c) and 3(g). The later measurements actually are similar to the dip-like feature

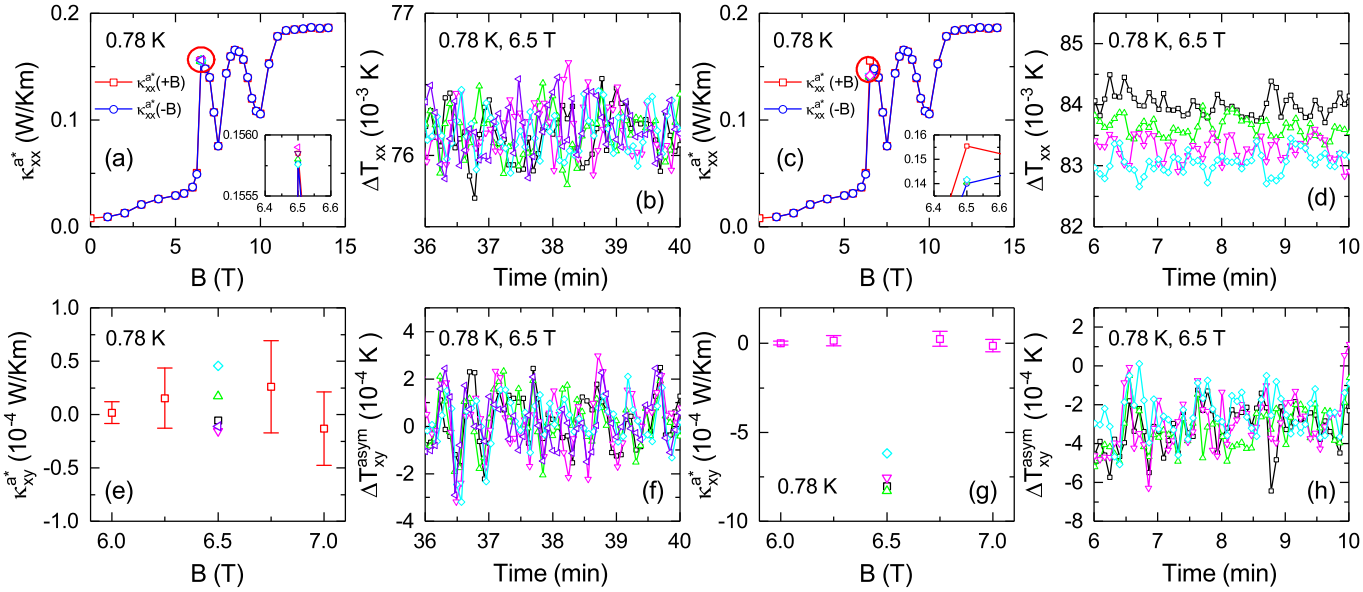


FIG. 3. (a,c) Magnetic field dependence of the longitudinal thermal conductivity κ^{a*}_{xx} for $+B$ (red open squares) and $-B$ (other symbols) at 0.78 K. The insets in (a) and (c) show the data at B_{a*1}. (e,g) Thermal Hall conductivity κ^{a*}_{xy} for $+B$ (red open squares) and $-B$ (other symbols) at 0.78 K. In panel (a), several repeated measurements gave indistinguishable $\kappa^{a*}_{xx}(B)$ values at B_{a*1} and corresponding small κ^{a*}_{xy} values, as indicated by the open symbols without line in panel (e). However, in panel (c), several measurements gave small differences among $\kappa^{a*}_{xx}(B)$ at B_{a*1} and corresponding large negative values, as indicated by the open symbols without line in panel (g). (b,f) Longitudinal temperature difference ΔT_{xx} and transverse temperature difference ΔT^{asym}_{xy} as a function of time that correspond to panels (a) and (e), respectively. (d,h) Longitudinal temperature difference ΔT_{xx} and transverse temperature difference ΔT^{asym}_{xy} as a function of time that correspond to panels (c) and (g), respectively. The difference between the measurements of (a,e) and those of (c,g) is that for the former ones the data were recorded after long time ($>$ 30 minutes) waiting for achieving the steady state of heat flowing, while for the later ones the data were recorded after only several minutes. The resulted difference in the κ^{a*}_{xy} and κ^{a*}_{xy} is significant only at B_{a*1}.

at B_{a*1} observed by Takeda *et al.* [30]. Thus, it can be concluded that this dip-like feature is not intrinsic.

The planar thermal Hall conductivity and thermal conductivity were also measured with magnetic field and heat current along the a axis. As shown in Figs. 4(a-d), the longitudinal thermal conductivity $\kappa^{a}_{xx}(B)$ exhibit the similar behaviors to the previous ultralow temperature data [29]. With increasing field, the κ^{a}_{xx} firstly increases and arrives a maximum at $\sim$ 7.5 T, and then decreases and reaches a minimum at $B_{a1} \sim 9.75$ T, which is close to the spin polarization transition for $B \parallel a$. Above B_{a1}, the κ^{a}_{xx} quickly increases and finally saturates in the polarized state. However, another kink-like anomaly appears in $\kappa^{a}_{xx}(B)$ at 10.25–10.5 T, which is marked as B_{a2}. This anomaly is likely due to a unexplored field-induced magnetic transition. Since this anomaly becomes indistinguishable at temperatures above 2.25 K, it cannot be probed by earlier magnetization studies [26]. In addition, there is an obvious hysteresis between the increasing and decreasing field data for $B < B_{a1}$. The unusual hysteresis behavior for $B < B_{a1}$ may be related to the magnetic domains which can scatter phonons in $Na_2Co_2TeO_6$. We note that Hong *et al.* recently also measured the $\kappa^{a*}_{xx}(B)$ and $\kappa^{a}_{xx}(B)$ at ultralow temperatures but they only observed hysteresis in $\kappa^{a*}_{xx}(B)$ [31]. Although the reason for the difference between their data and ours is unclear now, the possibility of the misalignment of heat current and magnetic field for our $\kappa^{a}_{xx}(B)$ measurements can be excluded. The reason is simply due to the hysteresis loop exhibits very different behaviors between the a and $a*$-axis field. In particular, for the $a*$-axis field, the κ^{a*}_{xx} data with field increasing is smaller than those with field decreasing; while for the a-axis field, when the hysteresis loop appear, the κ^{a}_{xx} with field increasing is larger than those with field decreasing.

Figures 4(e-h) show the planar thermal Hall conductivity κ^{a}_{xy} as a function of magnetic field at the selected temperatures. The data at $B < B_{a1}$ are rather similar at all temperatures, that is, there is weak positive signal at low fields and negative signal at the intermediate fields. A sign change of κ^{a}_{xy} seems to occur at the peak field of $\kappa^{a}_{xx}(B)$. A peak-like behavior appears for $B_{a1} < B < B_{a2}$ at low temperatures and disappears at 2.25 and 3.2 K. Rather large signal was observed for $B > B_{a2}$: there is large positive signal accompanied with sign change at low temperatures, which evolutes into a large negative dip at 3.2 K. This high-field feature are rather similar between the present data and Takeda *et al.*'s data at low temperatures [30]. However, their data at high temperatures show positive signal for $B > B_{a2}$.

One of our main experimental results is that both the $a*$- and a-axis magnetic fields can induce planar magnetic

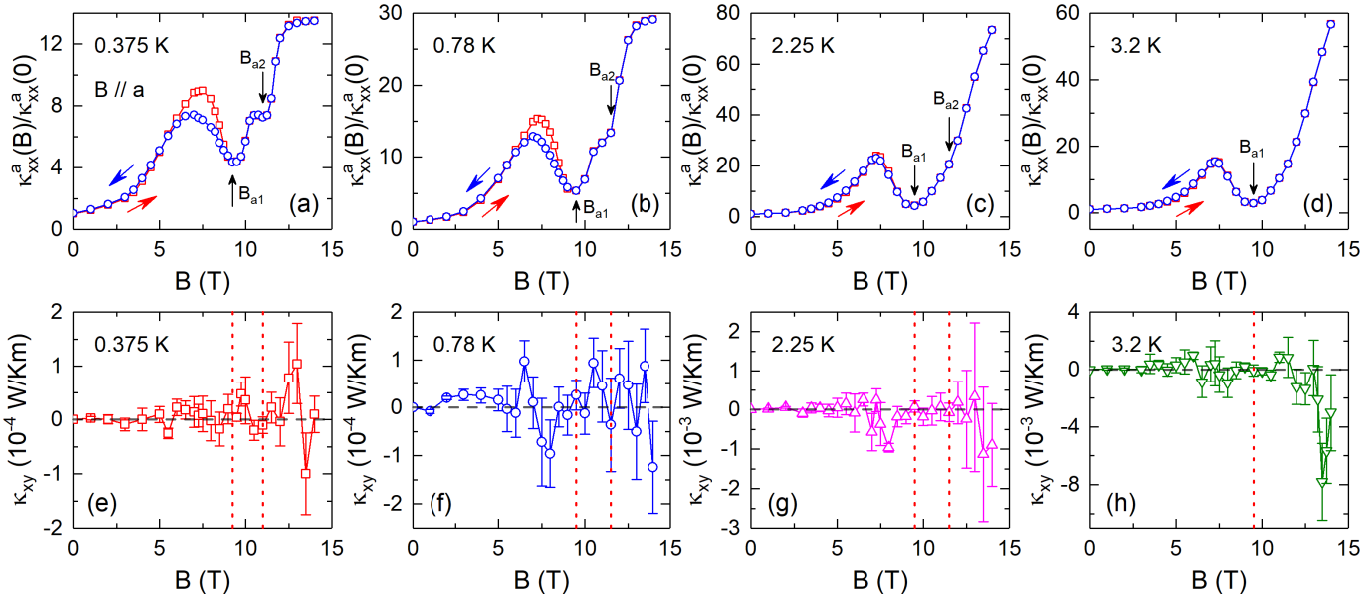


FIG. 4. Longitudinal thermal conductivity κ_{xx} and thermal Hall conductivity κ_{xy} of $Na_2Co_2TeO_6$ single crystals as a function of magnetic field with magnetic field and heat current applied along the a axis. (a-d) Isotherms of the κ_{xx} with respect to the zero-field value as a function of the magnetic field at 0.375, 0.78, 2.25 and 3.2 K, respectively. The red and blue arrows indicate the process of applying magnetic field, and an obvious hysteresis can be observed below B_{a1}. Black arrows indicate the critical fields as mentioned in main text. (e-h) Magnetic field dependence of thermal Hall conductivity κ_{xy} at different selected temperatures at 0.375, 0.78, 2.25, and 3.2 K, respectively. At each temperature the measurements were repeated more than five times to get the averaged data and error bars. The red dot line indicates the critical fields of magnetic transitions.

Hall effect in $Na_2Co_2TeO_6$ at low temperatures. This essentially reproduces the previous results from Takeda *et al.* [30], which were explained to be originated from the topological magnons. However, there are some obvious difference in the $\kappa_{xy}(B)$ between two groups' results. First, Takeda *et al.*'s results indicated that the planar Hall effect is closely correlated to the field-induced magnetic transitions. In contrast, our data indicate that the planar thermal Hall conductivity does not show up at the magnetic transition fields for both $B \parallel a*$ and $B \parallel a$. In particular, the most striking feature in Takeda *et al.*'s data is the sharp dip of $\kappa^{a*}_{xy}(B)$ data at B_{a*1}, which however was proved to be artificial by our careful checking on the relaxation time. This kind of difference suggests that the origin of the planar thermal Hall effect in $Na_2Co_2TeO_6$ needs further experimental investigations. Second, although both groups' data confirmed the quite large planar thermal Hall conductivity at high fields, there exist rather clear difference in the details like the sign change of $\kappa_{xy}(B)$. Another main result is that our thermal conductivity data $\kappa_{xx}(B)$ display much sharper anomalies at the field-induced magnetic transitions, which allows us to observe an additional kink-like anomaly in the $\kappa_{xx}(B)$ curves with $B \parallel a$. This indicates that there is likely another unexplored field-induced magnetic transition at B_{a2}. Therefore, the magnetic phase diagram of $Na_2Co_2TeO_6$ may be more complicated than what people have known.

We also note another recent study on the planar thermal Hall effect in $Na_2Co_2TeO_6$, reported by Chen *et al* [32]. In this work, the experiments were performed at higher temperature range of 4 – 100 K and the main finding is the non-zero κ_{xy} for either $B \parallel a*$ or $B \parallel a$. To compare our experimental results with Chen *et al.*'s, we also carried out the κ_{xy} measurement at higher temperature of 7.8 K and found pronounced κ_{xy} signals at high fields (see the Supplemental Material). Therefore, the planar thermal Hall effect was confirmed by at least three groups. We need to point out that this phenomenon is surprising. Theoretically, the non-zero κ_{xy} is not allowed for either $B \parallel a*$ or $B \parallel a$ because the crystal structure of $Na_2Co_2TeO_6$ (space group $P6_322$) has the C_2 rotational symmetry along both the $a*$ and a directions [6, 33–35]. Takeda *et al.* supposed that probably the presence of a magnetically ordered state breaks this two-fold rotation symmetry and allows this thermal Hall signal [30], while Chen *et al.* suggested that it may be due to a local symmetry breaking induced by some extrinsic effects [32]. At present, the underlying mechanism of this interesting result is still an open question and needs further explorations.

Here we give more discussion about the indication of the experimental results of κ_{xx} and κ_{xy} for the fields along different in-plane directions. Unlike the κ_{xx} result, the κ_{xy} reveals the wavefunction properties or Berry curvature properties of the relevant heat carriers, such as the magnetic excitations and/or the phonon modes. While the κ_{xy} is also sensitive to the density of carriers' states

and their mutual scattering like κ_{xx}, the Berry curvature properties can bring extra features such as the large change in the magnitude and the sign reversal to the κ_{xy}. This phenomenon occurs when the bands of the excitations experience radical changes in their Berry curvature distributions. For example, the excited magnon bands touch and reopen with a significant change of their Chern numbers. Actually, this change does not have to be associated with a magnetic structure transition. The magnetic structure can be smoothly varied by the external magnetic field without experiencing any phase transition while the change of magnon band structure topology can occur with a large change in κ_{xy} [36, 37]. Thus, the κ_{xy} provides more information about the properties of the excitations in the system. In Figs. 2 and 4, as we have previously mentioned, at the magnetic transitions that are indicated in the κ_{xx}, there are the associated changes in the κ_{xy} if the signal is discernible. Nevertheless, the κ_{xy} still experience sign reversals or large magnitude change at the magnetic fields where there are no obvious signatures in the κ_{xx}. This is clearly observed in Fig. 2 for $B > B_{a*3}$ and in Fig. 4 for $B > B_{a2}$. Thus, a radical change of the magnon band structure topology and the associated Berry curvature distribution may be experienced before the system enters a full polarized state. In fact, some recent theoretical researches have demonstrated that for the in-plane magnetic fields the thermal Hall conductivity of Kitaev magnets arises from the topological magnons with finite Chern numbers and a peculiar sign structure follows from the symmetries of the momentum space Berry curvature [33, 34]. This scenario is compatible with our reasoning above, and may be adopted to describe the planar thermal Hall effect of $Na_2Co_2TeO_6$, particularly the pronounced $\kappa_{xy}(B)$ in high-field region.

In addition to the properties about the magnetic excitations and magnetic structures in the fields, our results are quite indicative about the candidate model for $Na_2Co_2TeO_6$. The XXZ spin model that was recently proposed for the honeycomb cobalt $BaCo_2(AsO_4)_2$ has a global U(1) symmetry. This implies that the heat transport for the fields in the a and $a*$ directions should behave identically. Our experiments for $Na_2Co_2TeO_6$, however, show quite distinct behaviors for these two directions. This strongly indicates that the global U(1) symmetry should be absent for $Na_2Co_2TeO_6$. We thus think more anisotropic spin interactions should be included for understanding the physics of $Na_2Co_2TeO_6$. These results put some constraints on the candidate models for $Na_2Co_2TeO_6$.

IV. SUMMARY

In summary, we study both the in-plane thermal conductivity and thermal Hall conductivity of $Na_2Co_2TeO_6$ in magnetic fields along the honeycomb layer. It is found that the zero-field thermal conductivity displays weak in-plane anisotropy, while the magnetic fields along the a or $a*$ axis affect the κ_{xx} quite differently. The field-induced magnetic transitions induce anomalies at the low-temperature $\kappa^a_{xx}(B)$ and $\kappa^{a*}_{xx}(B)$ curves. Although most of these transitions have been probed by various experiments including thermal conductivity, the present $\kappa^a_{xx}(B)$ data for $B \parallel a$ reveal an unexplored magnetic transition at very low temperatures. Either the a-axis or the $a*$-axis magnetic fields can induce planar thermal Hall effect, which is mainly related to the magnon Berry curvature rather than the field-induced magnetic transitions. These results put clear constraints on the in-plane high-field phase of $Na_2Co_2TeO_6$ and the anisotropic spin interactions must be included in theoretical models.

ACKNOWLEDGMENTS

This work was supported by the National Natural Science Foundation of China (Grant Nos. 12274388, 12174361, 12104010, and 12104011), the Nature Science Foundation of Anhui Province (Grant Nos. 1908085MA09 and 2108085QA22), and the Research Grants Council of Hong Kong with C7012-21GF. The work at the University of Tennessee was supported by the NSF with Grant No. NSF-DMR-2003117.

[1] A. Kitaev, Anyons in an exactly solved model and beyond, Ann. Phys. **321**, 2 (2006).
[2] G. Jackeli and G. Khaliullin, Mott Insulators in the Strong Spin-Orbit Coupling Limit: From Heisenberg to a Quantum Compass and Kitaev Models, Phys. Rev. Lett. **102**, 017205 (2009).
[3] K. W. Plumb, J. P. Clancy, L. J. Sandilands, V. Vijay Shankar, Y. F. Hu, K. S. Burch, H.-Y. Kee, and Y.-J. Kim, α-$RuCl_3$: A spin-orbit assisted Mott insulator on a honeycomb lattice, Phys. Rev. B **90**, 041112(R) (2014).
[4] H. Takagi, T. Takayama, G. Jackeli, G. Khaliullin, and S. E. Nagler, Concept and realization of Kitaev quantum spin liquids, Nat. Rev. Phys. **1**, 264 (2019).
[5] Y. Kasahara, T. Ohnishi, Y. Mizukami, O. Tanaka, S. Ma, K. Sugii, N. Kurita, H. Tanaka, J. Nasu, Y. Motome, T. Shibauchi, and Y. Matsuda, Majorana quantization and half-integer thermal quantum Hall effect in a Kitaev spin liquid, Nature **559**, 227 (2018).
[6] T. Yokoi, S. Ma, Y. Kasahara, S. Kasahara, T. Shibauchi, N. Kurita, H. Tanaka, J. Nasu, Y. Motome, C. Hickey, S. Trebst, and Y. Matsuda, Half-integer quantized anomalous thermal Hall effect in the Kitaev material candidate α-$RuCl_3$, Science **373**, 568 (2021).
[7] J. A. N. Bruin, R. R. Claus, Y. Matsumoto, N. Kurita, H. Tanaka, and H. Takagi, Robustness of the thermal Hall effect close to half-quantization in α-$RuCl_3$, Nat. Phys.

18, 401 (2022).
[8] H. Liu and G. Khaliullin, Pseudospin exchange interactions in d^7 cobalt compounds: Possible realization of the Kitaev model, Phys. Rev. B **97**, 014407 (2018).
[9] R. Sano, Y. Kato, and Y. Motome, Kitaev-Heisenberg Hamiltonian for high-spin d^7 Mott insulators, Phys. Rev. B **97**, 014408 (2018).
[10] H. Liu, J. Chaloupka, and G. Khaliullin, Kitaev Spin Liquid in 3*d* Transition Metal Compounds, Phys. Rev. Lett. **125**, 047201 (2020).
[11] R. Zhong, T. Gao, N. P. Ong, and R. J. Cava, Weak-field induced nonmagnetic state in a Co-based honeycomb, Sci. Adv. **6**, eaay6953 (2020).
[12] T. Halloran, F. Desrochers, E. Z. Zhang, T. Chen, L. E. Chern, Z. Xu, B. Winn, M. Graves-Brook, M. B. Stone, A. I. Kolesnikov, Y. Qiu, R. Zhongg, R. Cava, Y. B. Kim, and C. Broholm, Geometrical frustration versus Kitaev interactions in $BaCo_2(AsO_4)_2$, PNAS **120**, e2215509119 (2023).
[13] S. Das, S. Voleti, T. Saha-Dasgupta, and A. Paramekanti, XY magnetism, Kitaev exchange, and long-range frustration in the $J_{\rm eff} = \frac{1}{2}$ honeycomb cobaltates, Phys. Rev. B **104**, 134425 (2021).
[14] M. Songvilay, J. Robert, S. Petit, J. A. Rodriguez-Rivera, W. D. Ratcliff, F. Damay, V. Balédent, M. Jiménez-Ruiz, P. Lejay, E. Pachoud, A. Hadj-Azzem, V. Simonet, and C. Stock, Kitaev interactions in the Co honeycomb antiferromagnets $Na_3Co_2SbO_6$ and $Na_2Co_2TeO_6$, Phys. Rev. B **102**, 224429 (2020).
[15] G. Lin, J. Jeong, C. Kim, Y. Wang, Q. Huang, T. Masuda, S. Asai, S. Itoh, G. Günther, M. Russina, Z. Lu, J. Sheng, L. Wang, J. Wang, G. Wang, Q. Ren, C. Xi, W. Tong, L. Ling, Z. Liu, H. Zhou, X. Wang, J. G. Park, Y. Wan, and J. Ma, Field-Induced Quantum Spin Disordered State in Spin-1/2 Honeycomb Magnet $Na_2Co_2TeO_6$, Nat. Commun. **12**, 5559 (2021).
[16] C. Kim, J. Jeong, G. Lin, P.Park, T.Masuda, S. Asai, S. Itoh, H.-S. Kim, H. Zhou, J. Ma, and J.-G. Park, Antiferromagnetic Kitaev interaction in $J_{\rm eff} = 1/2$ cobalt honeycomb materials $Na_3Co_2SbO_6$ and $Na_2Co_2TeO_6$, J. Phys.: Condens. Matt. **34**, 045802 (2022).
[17] A. M. Samarakoon, Q. Chen, H.Zhou, and V. O. Garlea, Static and dynamic magnetic properties of honeycomb lattice antiferromagnets $Na_2M_2TeO_6$, M = Co and Ni, Phys. Rev. B **104**, 184415 (2021).
[18] A. L. Sanders, R. A. Mole, J. Liu, A. J. Brown, D. Yu, C. D. Ling, and S. Rachel, Dominant Kitaev interactions in the honeycomb materials $Na_3Co_2SbO_6$ and $Na_2Co_2TeO_6$, Phys. Rev. B **106**, 014413 (2022).
[19] W. Yao, K. Iida, K. Kamazawa, and Y. Li, Excitations in the Ordered and Paramagnetic States of Honeycomb Magnet $Na_2Co_2TeO_6$, Phys. Rev. Lett. **129**, 147202 (2022).
[20] G. Xiao, Z. Xia, W. Zhang, X. Yue, S. Huang, X. Zhang, F. Yang, Y. Song, M. Wei, H. Deng, and D. Jiang, Crystal Growth and the Magnetic Properties of $Na_2Co_2TeO_6$ with Quasi-Two-Dimensional Honeycomb Lattice, Cryst. Growth Des. **19**, 2658 (2019).
[21] N. Li, R. R. Neumann, S. K. Guang, Q. Huang, J. Liu, K. Xia, X. Y. Yue, Y. Sun, Y. Y. Wang, Q. J. Li, Y. Jiang, J. Fang, Z. Jiang, X. Zhao, A. Mook, J. Henk, I. Mertig, H. D. Zhou, and X. F. Sun, Magnon-Polaron Driven Thermal Hall Effect in a Heisenberg-Kitaev Antiferromagnet, arXiv:2201.11396 (2022).
[22] E. Lefrançois, M. Songvilay, J. Robert, G. Nataf, E. Jordan, L. Chaix, C. V. Colin, P. Lejay, A. Hadj-Azzem, R. Ballou, and V. Simonet, Magnetic properties of the honeycomb oxide $Na_2Co_2TeO_6$, Phys. Rev. B **94**, 214416 (2016).
[23] A. K. Bera, S. M. Yusuf, A. Kumar, and C. Ritter, Zigzag antiferromagnetic ground state with anisotropic correlation lengths in the quasi-two-dimensional honeycomb lattice compound $Na_2Co_2TeO_6$, Phys. Rev. B **95**, 094424 (2017).
[24] W. Chen, X. Li, Z. Hu, Z. Hu, L. Yue, R. Sutarto, F. He, K. Iida, K. Kamazawa, W. Yu, X. Lin, and Y. Li, Spin-orbit phase behavior of $Na_2Co_2TeO_6$ at low temperatures, Phys. Rev. B **103**, L180404 (2021).
[25] C. H. Lee, S. Lee, Y. S. Chio, Z. H. Jang, R. Kalaivanan, R. Sankar, and K.-Y. Chio, Multistage development of anisotropic magnetic correlations in the Co-based honeycomb lattice $Na_2Co_2TeO_6$, Phys. Rev. B **103**, 214447 (2021).
[26] X. Hong, M. Gillig, R. Hentrich, W. Yao, V. Kocsis, A. R. Witte, T. Schreiner, D. Baumann, N. Pérez, A. U. B. Wolter, Y. Li, B. Büchner, and C. Hess, Strongly scattered phonon heat transport of the candidate Kitaev material $Na_2Co_2TeO_6$, Phys. Rev. B **104**, 144426 (2021).
[27] W. Yao and Y. Li, Ferrimagnetism and anisotropic phase tunability by magnetic fields in $Na_2Co_2TeO_6$, Phys. Rev. B **101**, 085120 (2020).
[28] G. Lin, Q. Zhao, G. Li, M. Shu, Y. Ma, J. Jiao, Q. Huang, J. Sheng, A. Kolesnikov, L. Li, L. Wu, X. Wang, H. Zhou, Z. Liu, and J. Ma, Evidence for field induced quantum spin liquid behavior in a spin-1/2 honeycomb magnet, https://doi.org/10.21203/rs.3.rs-2034295/v1 (2022).
[29] S. K. Guang, N. Li, R. L. Luo, Q. Huang, Y. Y. Wang, X. Y. Yue, K. Xia, Q. J. Li, X. Zhao, G. Chen, H. D. Zhou, and X. F. Sun, Thermal transport of fractionalized antiferromagnetic and field-induced states in the Kitaev material $Na_2Co_2TeO_6$, Phys. Rev. B **107**, 184423 (2023).
[30] H. Takeda, J. Mai, M. Akazawa, K. Tamura, J. Yan, K. Moovendaran, K. Raju, R. Sankar, K.-Y. Choi, and M. Yamashita, Planar thermal Hall effects in the Kitaev spin liquid candidate, $Na_2Co_2TeO_6$, Phys. Rev. Res. **4**, L042035 (2022).
[31] X. Hong, M. Gillig, W. Yao, L. Janssen, V. Kocsis, S. Gass, Y. Li, A. U. B. Wolter, B. Büchner, and C. Hess, Phonon thermal transport shaped by strong spin-phonon scattering in a Kitaev material $Na_2Co_2TeO_6$, arXiv:2306.16963 (2023).
~~R. R. Neumann, A. Mook, J. Henk, and I. Mertig, Thermal Hall Effect of Magnons in Collinear Antiferromagnetic Insulators: Signatures of Magnetic and Topological Phase Transitions, Phys. Rev. Lett. 128, 117201 (2022).~~
~~X. T. Zhang, Y. H. Gao, and G. Chen, Thermal Hall effects in quantum magnets, arXiv:2305.04830 (2023)~~
[32] L. Chen, Étienne Lefrançois, A. Vallipuram, Q. Barthélemy, A. Ataei, W. Yao, Y. Li, and L. Taillefer, Planar thermal Hall effect from phonons in a Kitaev candidate material, arXiv:2309.17231 (2023).
[33] L. E. Chern, E. Z. Zhang, and Y. B. Kim, Sign Structure of Thermal Hall Conductivity and Topological Magnons for In-Plane Field Polarized Kitaev Magnets, Phys. Rev. Lett. **126**, 147201 (2021).

[34] E. Z. Zhang, L. E. Chern, and Y. B. Kim, Topological magnons for thermal Hall transport in frustrated magnets with bond-dependent interactions, Phys. Rev. B **103**, 174402 (2021).

[35] T. Kurumaji, Symmetry-based requirement for the measurement of electrical and thermal Hall conductivity under an in-plane magnetic field, Phys. Rev. Research **5**, 023138 (2023).

[36] R. R. Neumann, A. Mook, J. Henk, and I. Mertig, Thermal Hall Effect of Magnons in Collinear Antiferromagnetic Insulators: Signatures of Magnetic and Topological Phase Transitions, Phys. Rev. Lett. **128**, 117201 (2022).

[37] X.-T. Zhang, Y. H. Gao, and G. Chen, Thermal Hall effects in quantum magnets, arXiv:2305.04830 (2023).